Electronic Supplementary Material (ESI) for Physical Chemistry Chemical Physics.


# Role of Hydrogen Bonding in Bulk Aqueous Phase Decomposition, Complexation, and Covalent Hydration of Pyruvic Acid

## Supplementary Material-A

**Michael Dave P. Barquilla and Maricris L. Mayes***

Department of Chemistry and Biochemistry, University of Massachusetts Dartmouth, North Dartmouth, MA 02747, USA

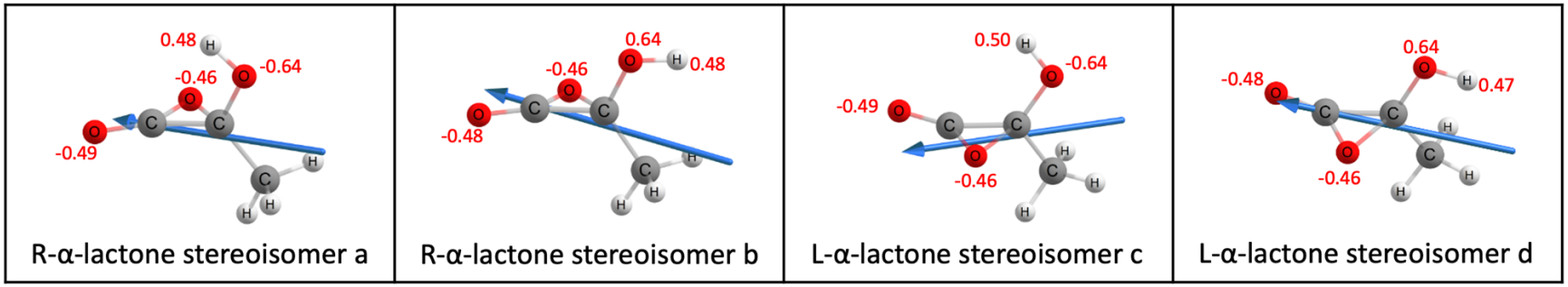


**Fig. S1A** Optimized structures of lactone isomers in gas[44] with dipole moments (blue arrows) and natural atomic charges (red), calculated at B2PLYP-D3BJ/aug-cc-pVTZ level of theory.

**Table S1A** Geometric features of pyruvic acid (PA) conformers and enol isomers in gas and aqueous phase (Fig. 1), calculated at B2PLYP-D3BJ/aug-cc-pVTZ level of theory. Bond distances are in angstroms (Å).

| Species | OH bond (carboxylic and alcoholic) | | C-OH bond (carboxylic) | | C=O bond (carboxylic) | | C=O bond (carbonyl) | | C-C bond | | H-bond | | OH-O Angle | |
|---|---|---|---|---|---|---|---|---|---|---|---|---|---|---|
| | Gas | Aq | Gas | Aq | Gas | Aq | Gas | Aq | Gas | Aq | Gas | Aq | Gas | Aq |
| Tc | 0.975 | 0.976 | 1.334 | 1.325 | 1.203 | 1.210 | 1.215 | 1.216 | 1.543 | 1.543 | 2.0223 | 2.0616 | 118.23 | 115.61 |
| Tt | 0.969 | 0.972 | 1.338 | 1.326 | 1.208 | 1.212 | 1.207 | 1.213 | 1.543 | 1.543 | 2.3090 | 2.3409 | 74.70 | 72.84 |
| Ct | 0.969 | 0.973 | 1.354 | 1.327 | 1.199 | 1.209 | 1.206 | 1.212 | 1.550 | 1.548 | 2.3128 | 2.3427 | 74.60 | 72.56 |
| | | | | | | | C-OH bond (alc.*) | | | | | | | |
| $enol_a$ | 0.968 | 0.971 | 1.342 | 1.329 | 1.215 | 1.220 | - | - | 1.485 | 1.487 | 2.2991 | 2.3312 | 75.20 | 73.40 |
| alc.* | 0.970 | 0.971 | - | - | - | - | 1.354 | 1.359 | - | - | 2.0691 | 2.0966 | 116.79 | 115.31 |
| $enol_b$ | 0.964 | 0.968 | 1.341 | 1.330 | 1.209 | 1.218 | - | - | 1.499 | 1.492 | - | - | - | - |
| alc.* | 0.972 | 0.971 | - | - | - | - | 1.348 | 1.358 | - | - | 2.0105 | 2.0701 | 118.07 | 115.87 |
| $enol_c$ | 0.964 | 0.967 | 1.355 | 1.337 | 1.198 | 1.213 | - | - | 1.506 | 1.493 | - | - | - | - |
| alc.* | 0.964 | 0.967 | - | - | - | - | 1.352 | 1.359 | - | - | - | - | - | - |
| $enol_d$ | 0.968 | 0.971 | 1.354 | 1.336 | 1.205 | 1.216 | - | - | 1.492 | 1.489 | 2.2782 | 2.3085 | 76.11 | 74.21 |
| alc.* | 0.963 | 0.966 | - | - | - | - | 1.358 | 1.361 | - | - | - | - | - | - |
| $enol_e$ | 0.968 | 0.971 | 1.346 | 1.335 | 1.208 | 1.216 | - | - | 1.494 | 1.491 | 2.2794 | 2.3092 | 75.91 | 74.07 |
| alc.* | 0.963 | 0.967 | - | - | - | - | 1.361 | 1.361 | - | - | - | - | - | - |
| $enol_f$ | 0.968 | 0.972 | 1.347 | 1.336 | 1.202 | 1.214 | - | - | 1.501 | 1.493 | - | - | - | - |
| alc.* | 0.963 | 0.967 | - | - | - | - | 1.373 | 1.364 | - | - | 1.9779 | 1.9938 | 117.94 | 116.09 |

** refers to alcoholic OH group on enol isomers (highlighted)*

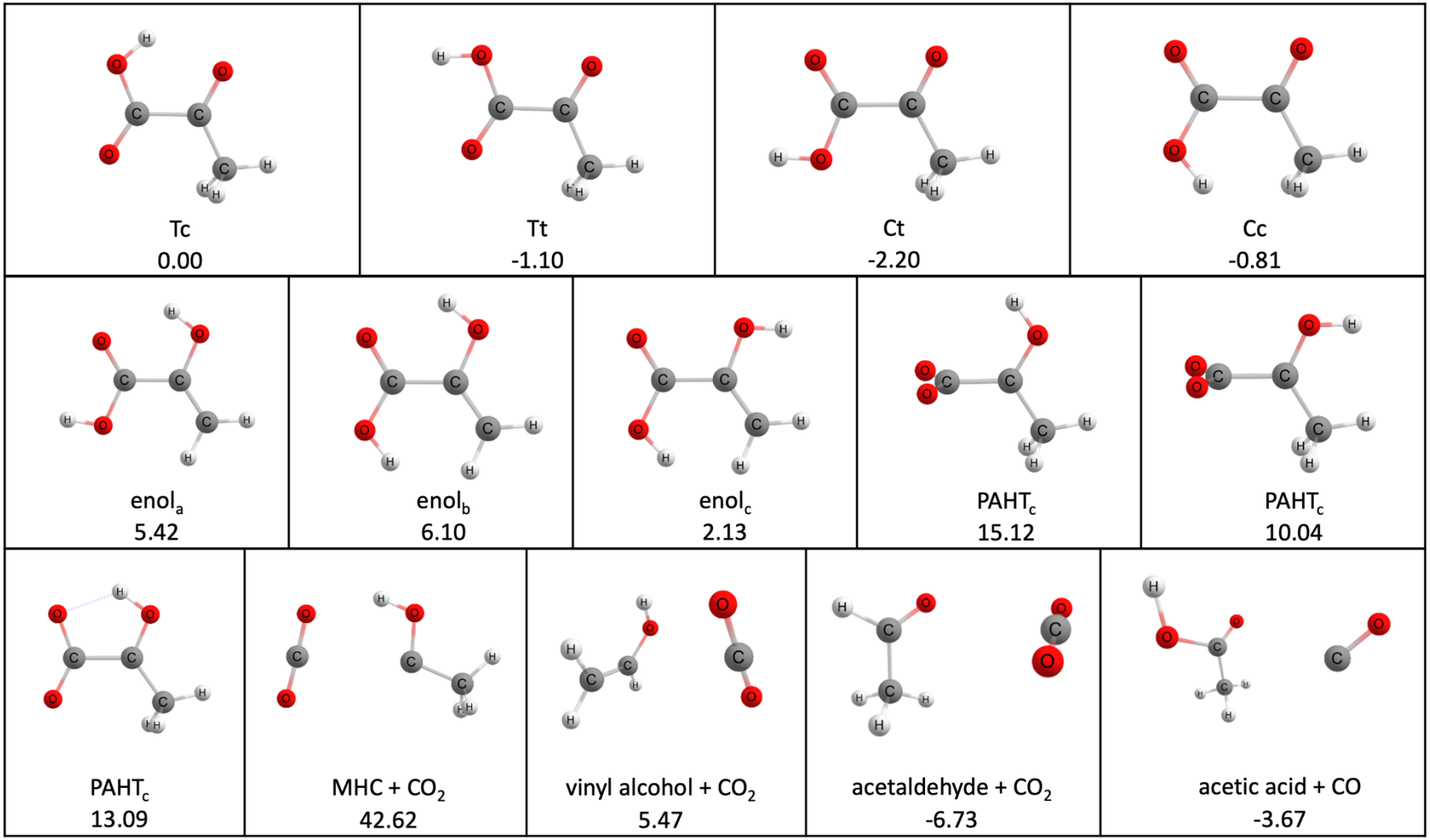


**Fig. S2A** Optimized structures and relative energies of the minima on the potential energy surface of pyruvic acid (PA) degradation (Fig. 2), calculated at SMD-CCSD(T)-F12/aug-cc-pVDZ-F12//SMD-B2PLYP-D3BJ/aug-cc-pVTZ level of theory. Relative energies (kcal/mol) with respect to Tc in aqueous phase.

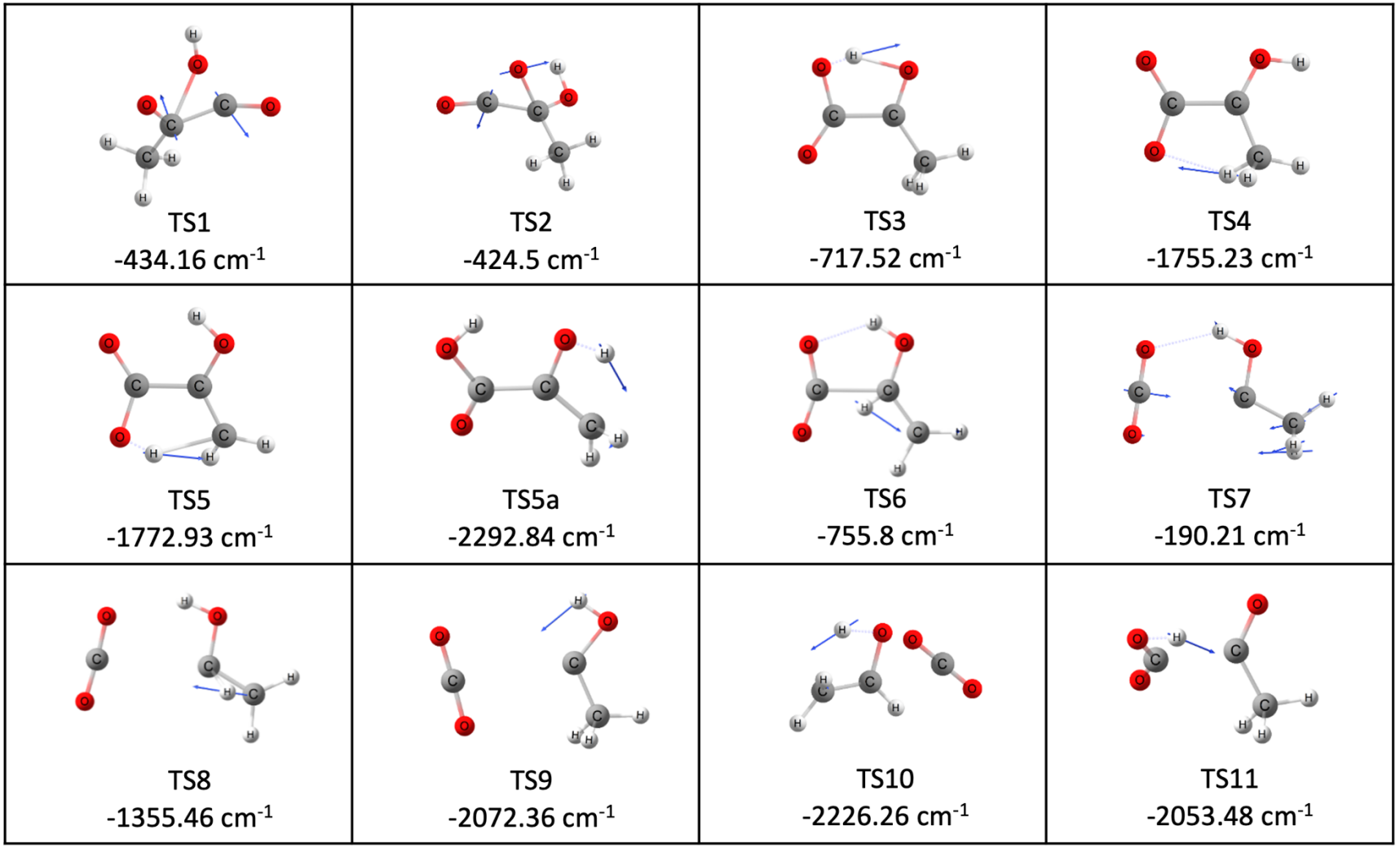


**Fig. S3A** Optimized structures for transition states identified in Scheme 1 and Fig. 2, with the corresponding imaginary frequencies in aqueous, calculated at SMD-B2PLYP-D3BJ/aug-cc-pVTZ level of theory. TS5a is an alternative TS from Tc to $enol_f$ via a hydride shift from the methyl group to carbonyl oxygen.

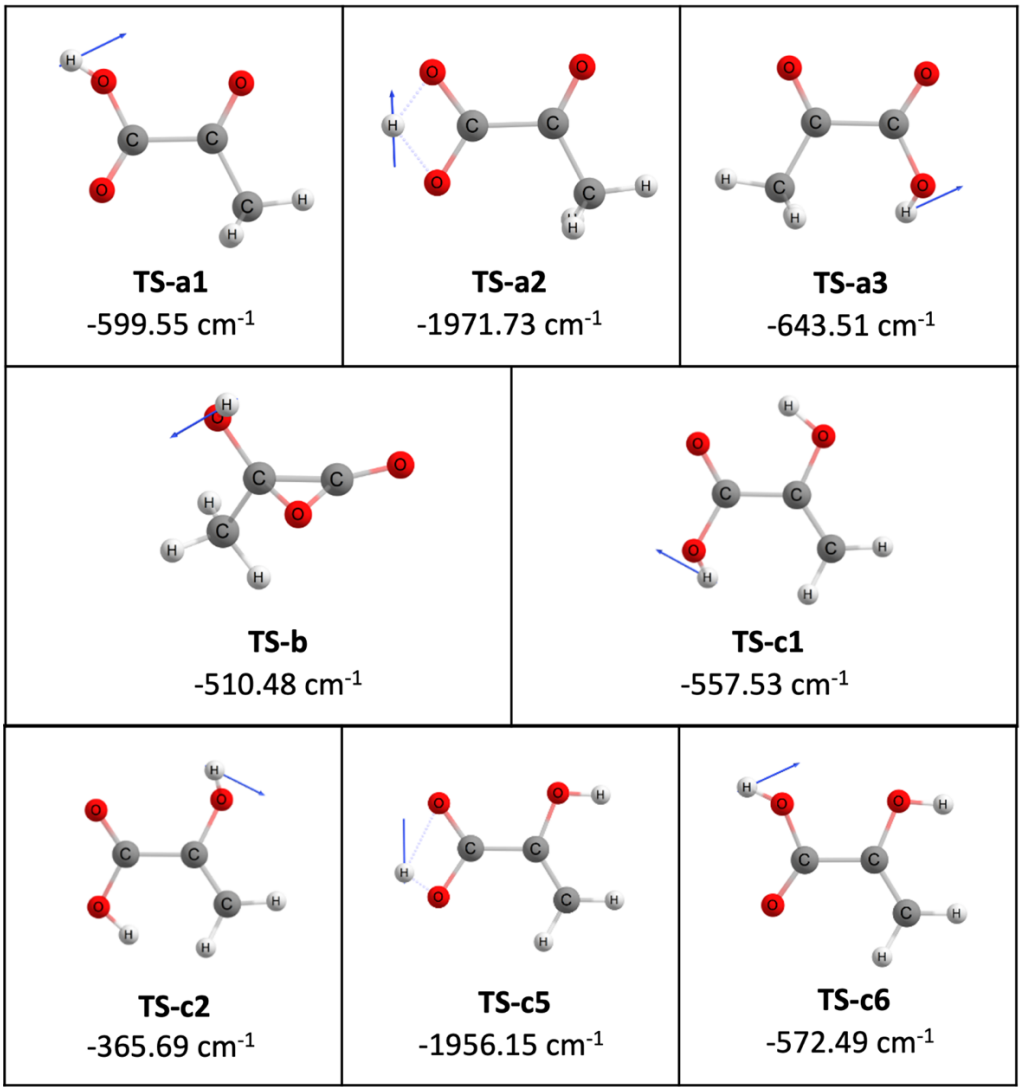


**Fig. S4A** Optimized structures of the transition states of conformational switching between pyruvic acid (PA) conformers, PA hydrogen-transferred (PAHT) tautomers and enol isomers found along the PA aqueous potential energy surface degradation, using SMD-B2PLYP-D3BJ/aug-cc-pVTZ. Indicated are the imaginary frequencies of the transition states in aqueous phase.

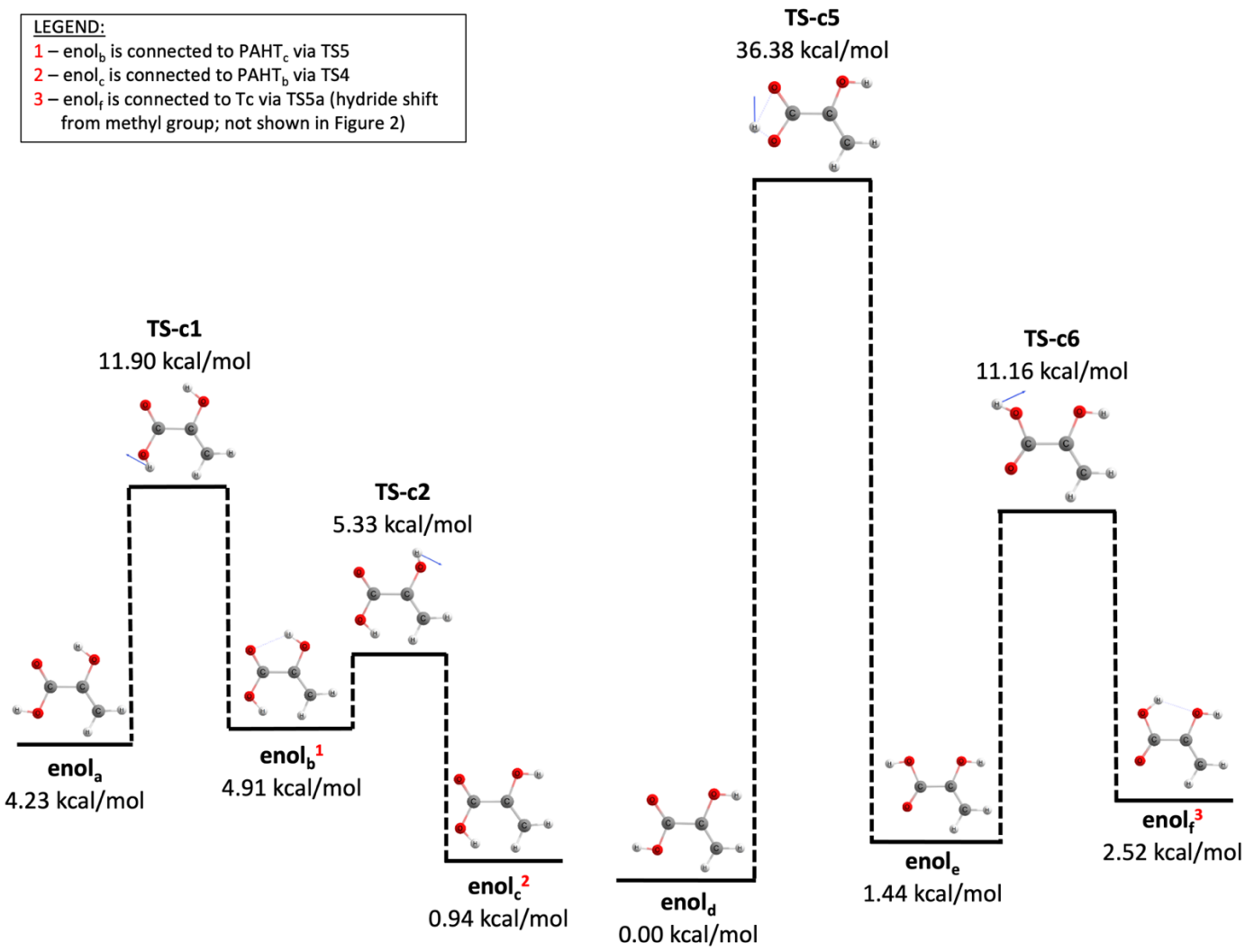


**Fig. S5A** Interconversion of enol isomers in aqueous phase. Unlike the gas phase,[44] no transition states were found for enol$_c$-enol$_d$ and enol$_a$-enol$_d$ switching. Indicated energies are relative to enol$_d$ and calculated using SMD-CCSD(T)-F12/aug-cc-pVDZ-F12//SMD-B2PLYP-D3BJ/aug-cc-pVTZ .

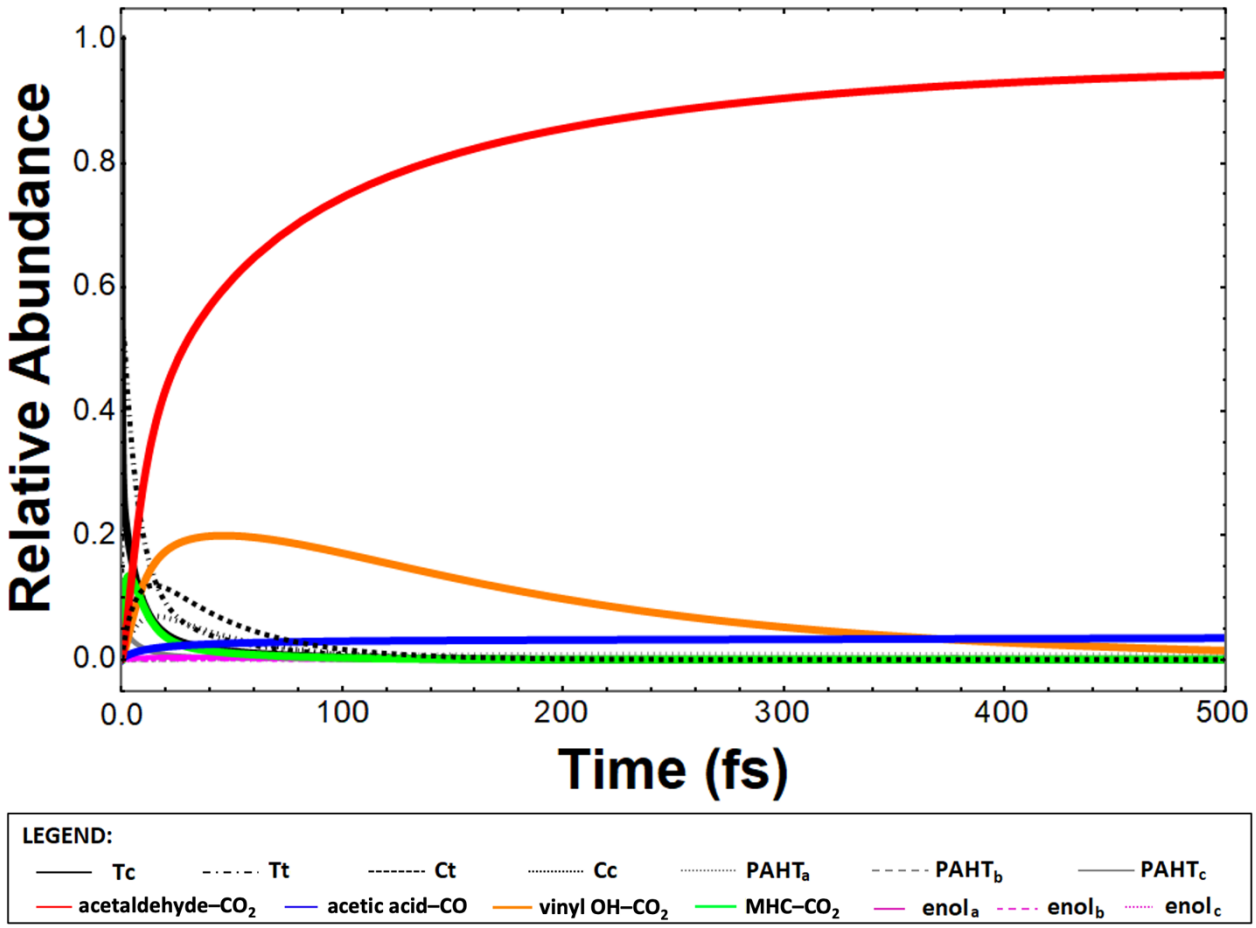


**Fig. S6A** Temporal dependence of pyruvic acid (PA) degradation species concentration in aqueous phase at 54 800 $cm^{-1}$ energy input and extended to 500 fs timescale. Calculations used RRKM microcanonical coefficients from SMD-CCSD(T)-F12/aug-cc-pVDZ-F12 single point energies and SMD-B2PLYP-D3BJ/aug-cc-pVTZ frequencies.

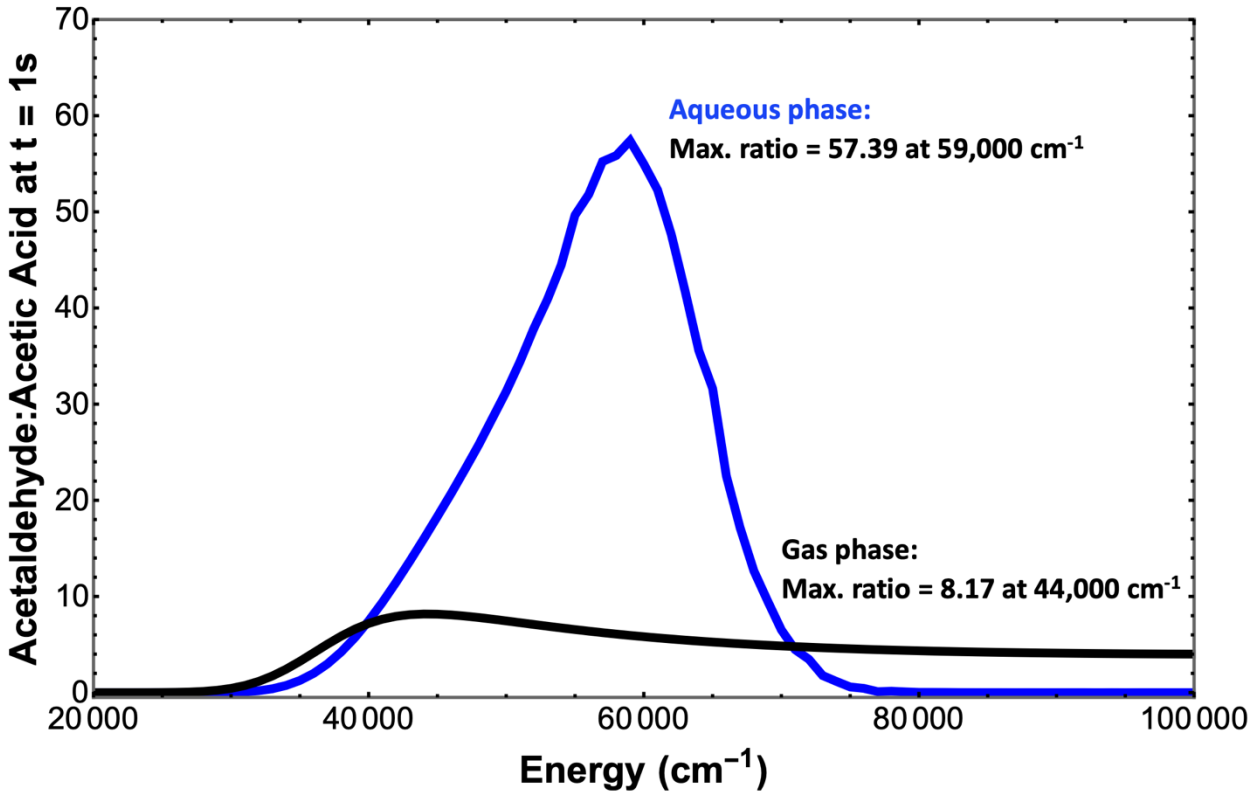


**Fig. S7A** Ratios of acetaldehyde to acetic acid in aqueous phase and previous gas phase calculations,[44] determined at reaction completion (t = 1 sec) within 20 000 $cm^{-1}$ to 100 000 $cm^{-1}$. Calculations used RRKM microcanonical coefficients from SMD-CCSD(T)-F12/aug-cc-pVDZ-F12 single point energies and SMD-B2PLYP-D3BJ/aug-cc-pVTZ frequencies.

**Table S2A** Calculated parameters of the least-square fit of the Arrhenius plot of pyruvic acid direct decomposition (Fig. 4), 2,2-dihydroxypropanoic acid (DHPA) and DHPA–$H_2O$ reaction rate coefficients (Fig. 6) in aqueous phase. The three-parameter Arrhenius equation is $k(T) = A\,T^n\,e^{-E_A/RT}$ and the rate coefficients (k) are calculated from SMD-CCSD(T)-F12/aug-cc-pVDZ-F12 single point energies and SMD-B2PLYP-D3BJ/aug-cc-pVTZ frequencies.

| **Reaction** | **Method** | **A** ($s^{-1}$) | **n** | **$E_A$** (kcal/mol) |
|---|---|---|---|---|
| Tc → acetic acid + CO (gas)[a] | RRKM ($N_2$) | 3.043 x $10^{10}$ | 0.90 | 54.58 |
| Tc → acetic acid + CO (TS1) | RRKM ($H_2O$) | 6.09 x $10^{10}$ | 0.82 | 52.01 |
| Tc → $PAHT_c$ (TS3) | RRKM ($H_2O$) | 3.761 x $10^{35}$ | -7.28 | 19.45 |
| Tc → Tt (TS-a1) | RRKM ($H_2O$) | 5.563 x $10^{33}$ | -6.98 | 14.30 |
| Tc → MHC–$CO_2$ (gas)[a] | RRKM ($N_2$) | 1.574 x $10^{13}$ | 0.15 | 41.03 |
| $PAHT_c$ → MHC–$CO_2$ (TS7) | RRKM ($H_2O$) | 2.863 x $10^{23}$ | -2.81 | 34.81 |
| Tc → acetaldehyde + $CO_2$ (gas)[a] | RRKM ($N_2$) | 1.717 x $10^{11}$ | 0.93 | 72.80 |
| Tc → acetaldehyde + $CO_2$ (TS11) | RRKM ($H_2O$) | 2.079 x $10^{11}$ | 0.94 | 75.60 |
| Tc → $PAHT_c$ (TS3) | RRKM ($H_2O$) | 3.761 x $10^{35}$ | -7.28 | 19.45 |
| | TST | 1.459 x $10^{13}$ | 0.11 | 13.48 |
| | TST w/ Wigner | 4.068 x $10^{12}$ | 0.26 | 13.03 |
| | TST w/ Eckart | 8.190 x $10^{12}$ | 0.17 | 13.43 |
| Tc–$H_2O_b$ → DHPA | TST | 4.452 x $10^{10}$ | -0.29 | 39.70 |
| | TST w/ Wigner | 1.074 x $10^{10}$ | -0.14 | 38.55 |
| | TST w/ Eckart | 4.510 x $10^{-1}$ | 2.96 | 33.31 |
| Tc–$H_2O_b$' → DHPA | TST w/ Eckart (gas)[a] | 1.226 x $10^{1}$ | 2.61 | 31.69 |
| Tc–$2H_2O$ → DHPA–$H_2O$ | TST | 5.430 x $10^{9}$ | -0.49 | 36.14 |
| | TST w/ Wigner | 1.221 x $10^{9}$ | -0.32 | 35.00 |
| | TST w/ Eckart | 4.121 x $10^{-1}$ | 2.50 | 30.21 |
| | TST w/ Eckart (gas)[a] | 8.574 x $10^{2}$ | 1.32 | 28.47 |

[a] *Ref. 44*

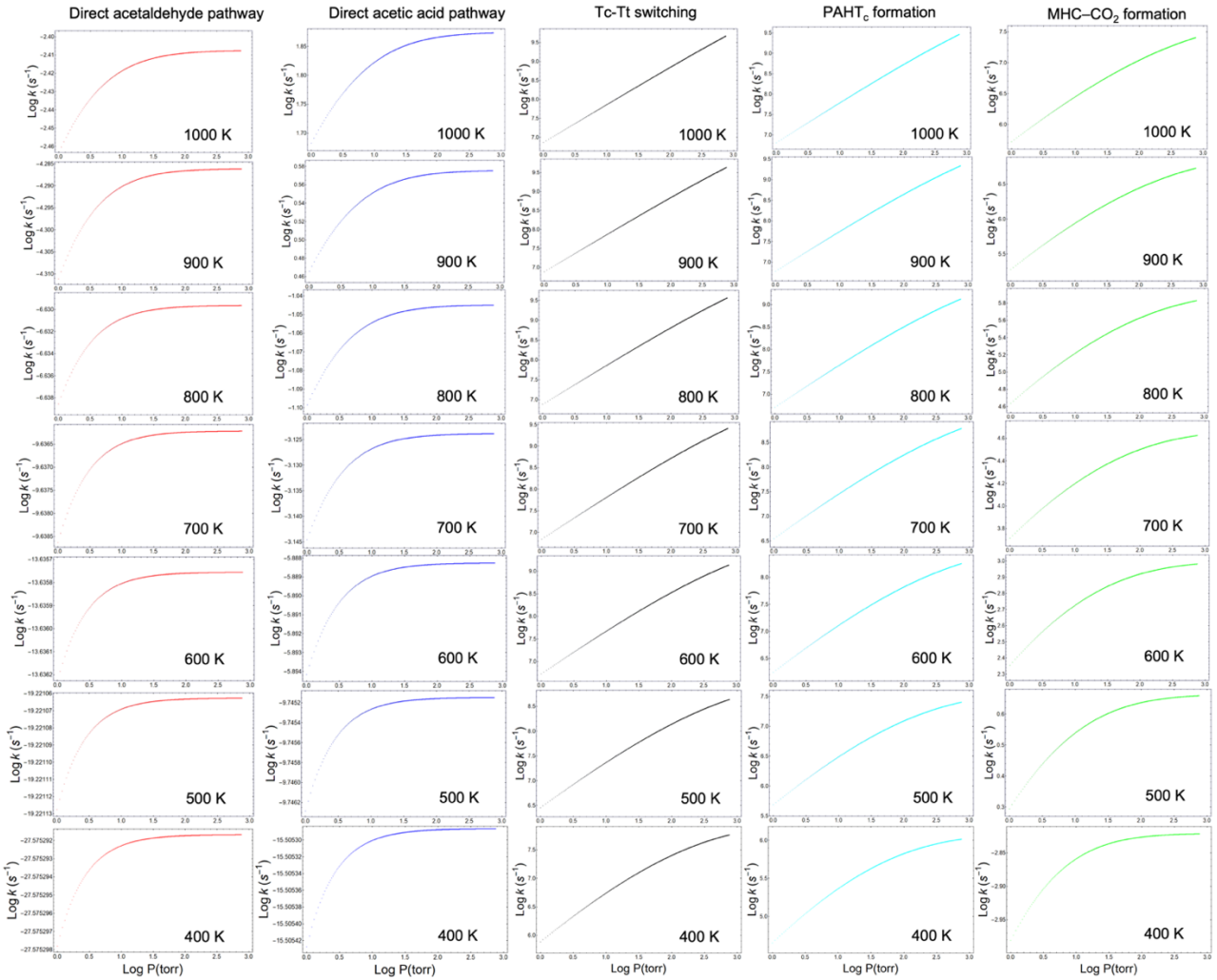


**Fig. S8A** Effect of pressure on the rates of all the direct pyruvic acid decomposition channels and MHC–$CO_2$ formation from $PAHT_c$ in aqueous phase. Pressure is evaluated between 1 to 760 torr at 0.10 torr increment for 400 K to 1000 K at 100 K interval and the RRKM rates (k) are calculated from SMD-CCSD(T)-F12/aug-cc-pVDZ-F12 single point energies and SMD-B2PLYP-D3BJ/aug-cc-pVTZ frequencies.

| | | |
|---|---|---|
| 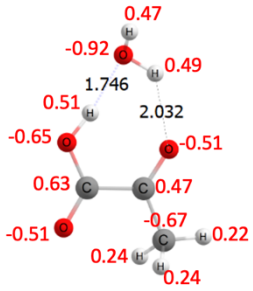 gas phase | ---- | 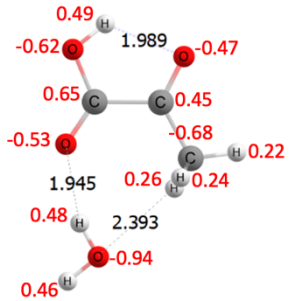 gas phase |
| 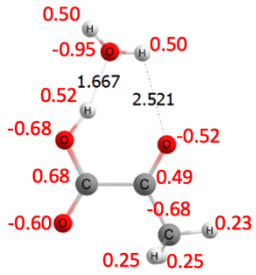 aqueous phase | 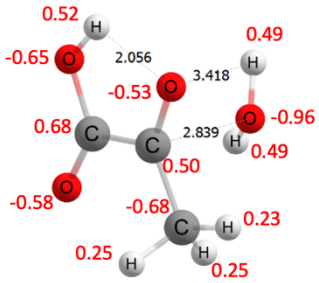 aqueous phase | 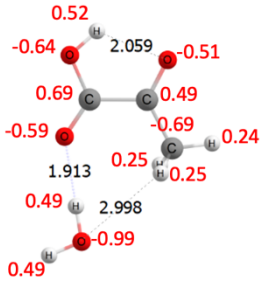 aqueous phase |
| **Tc–$H_2O_a$**<br>**($H_2O$---carboxyl and carbonyl group)** | **Tc–$H_2O_b$**<br>**($H_2O$---$C_{carboxyl}$-$C_{carbonyl}$ plane)** | **Tc–$H_2O_b$'**<br>**($H_2O$---carboxyl and methyl group)** |

**Fig. S9A** Tc monohydrates in gas and aqueous phase. Structures and NBO natural atomic charges (red) are calculated using B2PLYP-D3BJ/aug-cc-pVTZ. SMD was used for all aqueous phase calculations.

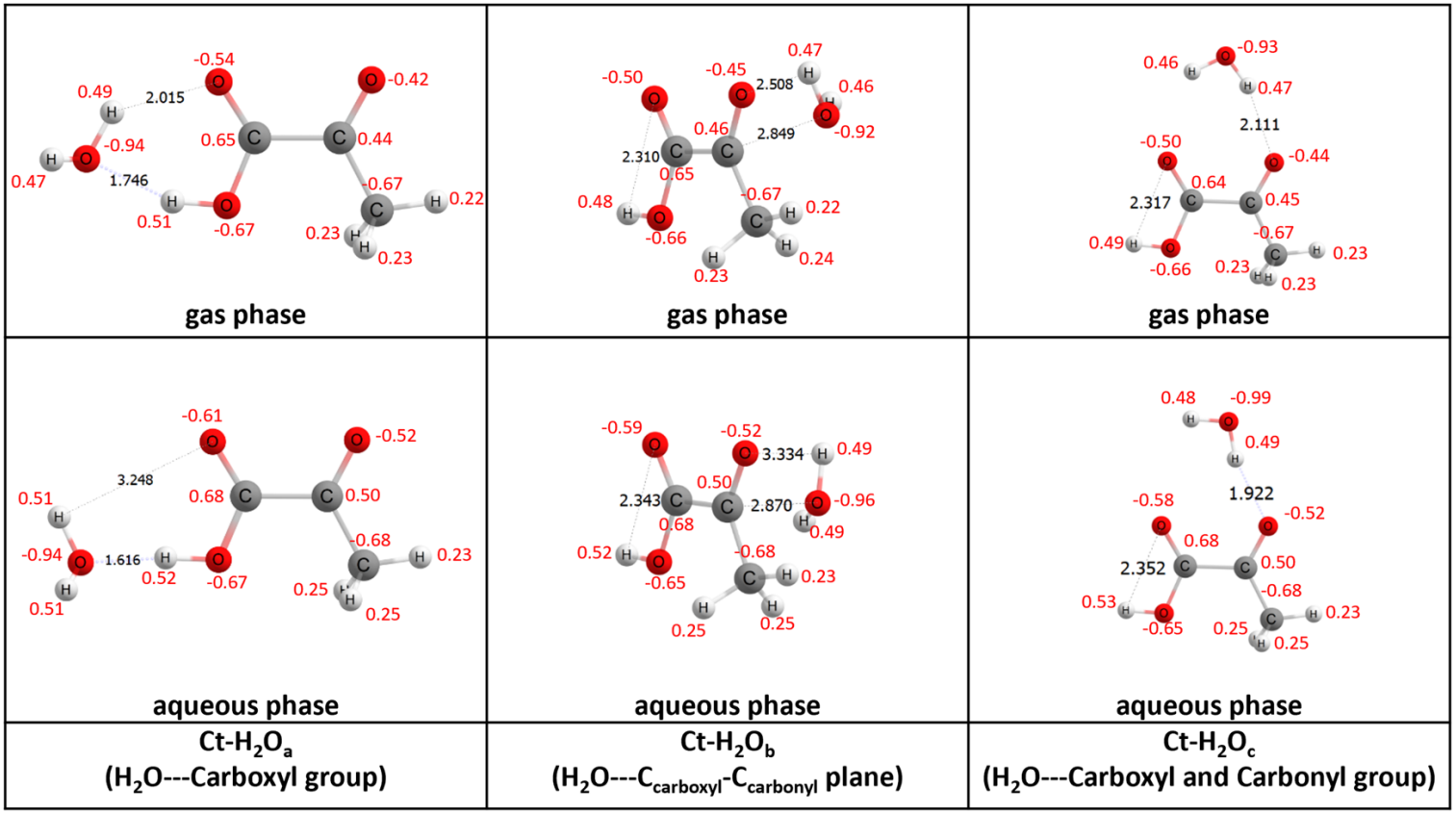


**Fig. S10A** Ct monohydrates in gas and aqueous phase. Structures and NBO natural atomic charges (red) are calculated using B2PLYP-D3BJ/aug-cc-pVTZ. SMD was used for all aqueous phase calculations.

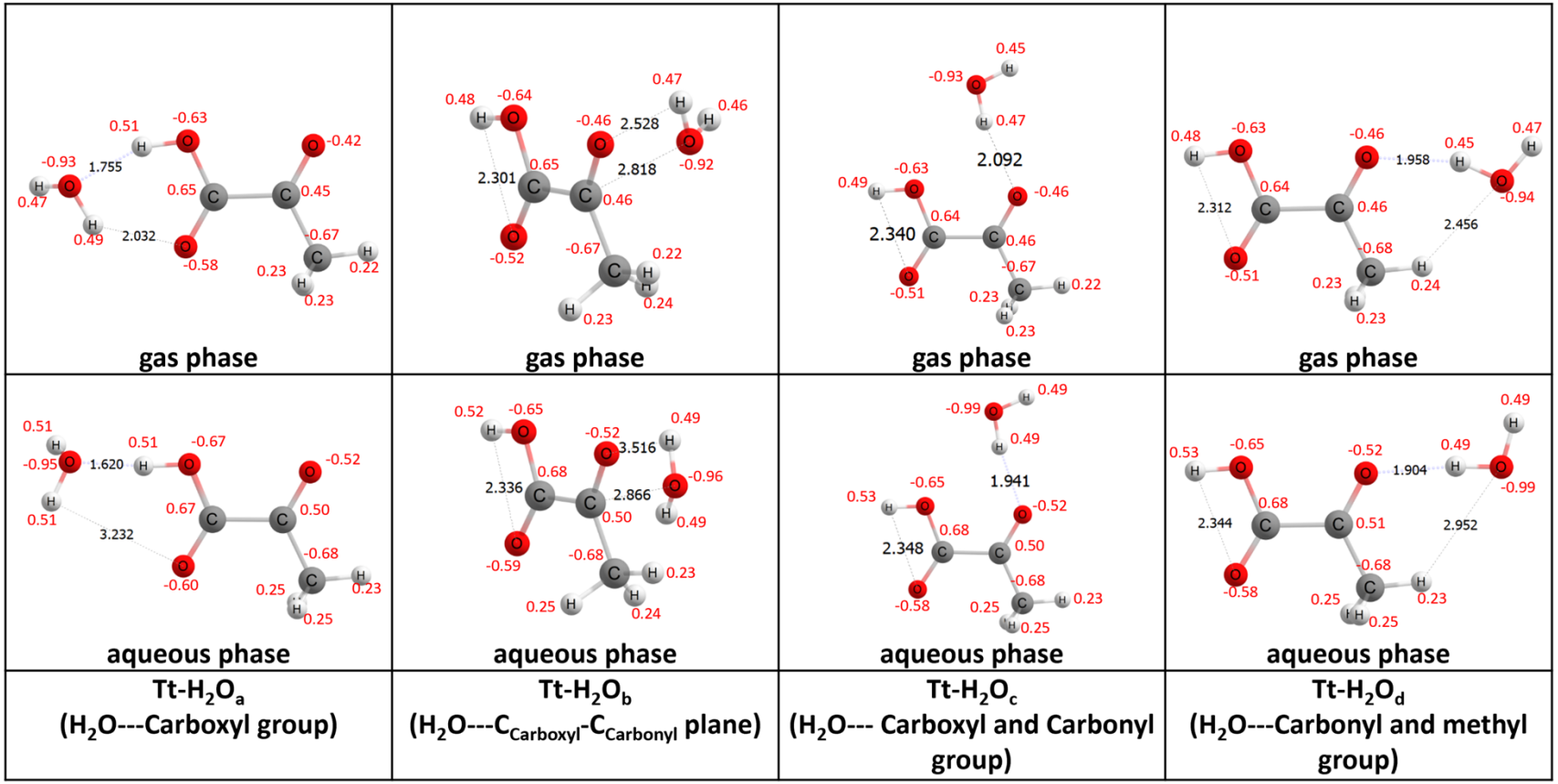


**Fig. S11A** Tt monohydrates in gas and aqueous phase. Structures and NBO natural atomic charges (red) are calculated using B2PLYP-D3BJ/aug-cc-pVTZ. SMD was used for all aqueous phase calculations.

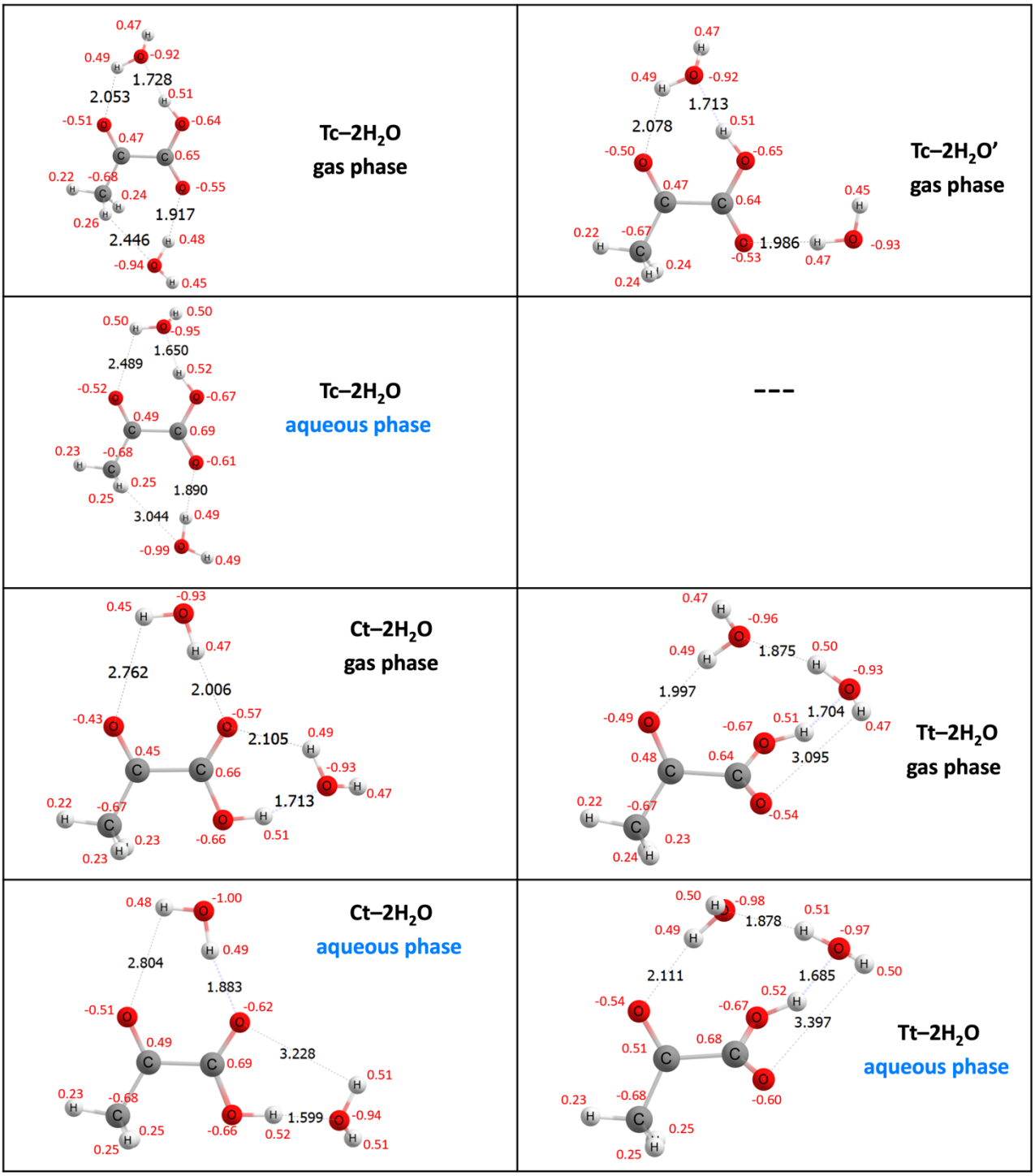


**Fig. S12A** PA dihydrates. Structures and NBO natural atomic charges (red) are calculated using B2PLYP-D3BJ/aug-cc-pVTZ. SMD was used for all aqueous phase calculations.

**Table S3A** Relative thermodynamic properties (kcal/mol) of PA and PA hydrates with respect to their lowest energy conformers, in gas and aqueous phase at 1 atm and 298.15 K, calculated at CCSD(T)-F12/aug-cc-pVDZ-F12//B2PLYP-D3/aug-cc-pVTZ level of theory. Aqueous phase calculations used SMD for the structure and energy correction.

| Species | | Gas phase | | | Aqueous phase | | | Intrinsic solvation |
|---|---|---|---|---|---|---|---|---|
| | | rel. $H^o_{gas}$ | rel. $-TS^o_{gas}$ | rel. $G^o_{gas}$ | rel. $H^o_{aq}$ | rel. $-TS^o_{aq}$ | rel. $G^o_{aq}$ | $\Delta G^o_{Sol}$ |
| PA | | | | | | | | |
| | Tc | 0.00 | 0.00 | 0.00 | 0.00 | 0.00 | 0.00 | -7.73 |
| | Ct | 4.28 | -0.88 | 3.40 | -2.15 | -0.10 | -2.25 | -13.37 |
| | Tt | 2.75 | -0.36 | 2.39 | -1.05 | -0.14 | -1.20 | -11.31 |
| PA monohydrated complexes | | | | | | | | |
| Tc | $Tc–H_2O_a$ | 0.00 | 0.00 | 0.00 | 0.00 | 0.00 | 0.00 | -16.50 |
| | $Tc–H_2O_b$ | - | - | - | 2.02 | -1.05 | 0.97 | - |
| | $Tc–H_2O_b'$ | 1.47 | -0.65 | 0.82 | 7.26 | -0.73 | 6.53 | -10.79 |
| Ct | $Ct–H_2O_a$ | 1.07 | 0.10 | 1.17 | -2.28 | -0.52 | -2.80 | -20.47 |
| | $Ct–H_2O_b$ | 6.44 | -1.45 | 4.99 | -0.24 | -1.33 | -1.57 | -23.06 |
| | $Ct–H_2O_c$ | 6.53 | -1.53 | 5.00 | 5.21 | -1.11 | 4.10 | -17.40 |
| Tt | $Tt–H_2O_a$ | 0.19 | 0.16 | 0.35 | -2.34 | -0.52 | -2.87 | -19.71 |
| | $Tt–H_2O_b$ | 5.45 | -1.45 | 4.00 | 0.39 | -1.10 | -0.71 | -21.21 |
| | $Tt–H_2O_c$ | 4.44 | -1.69 | 2.75 | 4.94 | -0.87 | 4.07 | -15.17 |
| | $Tt–H_2O_d$ | 5.00 | -1.68 | 3.32 | 5.69 | -1.33 | 4.36 | -15.45 |
| PA dihydrated complexes | | | | | | | | |
| | $Tc–2H_2O$ | 0.00 | 0.00 | 0.00 | 0.00 | 0.00 | 0.00 | -19.26 |
| | $Tc–2H_2O'$ | 1.47 | -0.77 | 0.71 | - | - | - | - |
| | $Ct–2H_2O$ | 1.59 | 0.23 | 1.82 | -2.80 | 0.97 | -1.83 | -22.91 |
| | $Tt–2H_2O$ | -1.03 | 1.30 | 0.26 | 0.53 | 0.11 | 0.64 | -18.88 |

[a] *Intrinsic Gibbs free energy of solvation:* $\Delta G^o_{Solv} = G^o_{aq} - G^o_{gas}$

**Table S4A** Geometric features and relative energies of PA-water complexes containing intermolecular H-bonds in gas and aqueous phase (Fig. S9A to S12A). Orientation b of PA-$H_2O$ complexes is not included since the only dominant interaction found is p-$\pi$*.

| Complex | H-bond location | Bond length, Å | | Δdistance[a], Å | OH-O angles | | Relative $G^o$ | |
|---|---|---|---|---|---|---|---|---|
| | | Gas | Aq | | Gas | Aq | Gas | Aq |
| PA-$H_2O$ | | | | | | | | |
| Tc–$H_2O_a$ | $OH_{Carboxylic}$–$O_{Water}$ | 1.746 | 1.667 | -0.079 | 171.10 | 162.05 | 0.00 | 0.00 |
| | $OH_{Water}$–$O_{Carbonyl}$ | 2.032 | 2.521 | 0.489 | 131.07 | 103.65 | | |
| Tc–$H_2O_b$' | $O_{Carboxylic}$–$HO_{Water}$ | 1.945 | 1.913 | -0.032 | 161.13 | 178.93 | 0.82 | 6.53 |
| | $O_{Water}$–$HC_{Methyl}$ | 2.393 | 2.998 | 0.605 | 131.98 | 108.99 | | |
| Ct–$H_2O_a$ | $OH_{Carboxylic}$–$O_{Water}$ | 1.746 | 1.616 | -0.130 | 157.65 | 174.65 | 1.17 | -2.80 |
| | $O_{Carboxylic}$–$HO_{Water}$ | 2.015 | 3.248 | 1.233 | 134.33 | 90.77 | | |
| Ct–$H_2O_c$ | $O_{Carbonyl}$–$HO_{Water}$ | 2.111 | 1.922 | -0.189 | 162.33 | 164.28 | 5.00 | 4.10 |
| | $O_{Carboxylic}$–$HO_{Water}$ | 2.410 | 2.843 | 0.433 | 130.10 | 101.35 | | |
| Tt–$H_2O_a$ | $OH_{Carboxylic}$–$O_{Water}$ | 1.755 | 1.620 | -0.135 | 158.11 | 174.66 | 0.35 | -2.87 |
| | $O_{Carboxylic}$–$HO_{Water}$ | 2.032 | 3.232 | 1.200 | 133.78 | 91.05 | | |
| Tt–$H_2O_c$ | $O_{Carbonyl}$–$HO_{Water}$ | 2.092 | 1.941 | -0.151 | 162.54 | 170.33 | 2.75 | 4.07 |
| Tt-$H_2O_d$ | $O_{Carbonyl}$–$HO_{Water}$ | 1.958 | 1.904 | -0.054 | 157.99 | 174.60 | 3.32 | 4.36 |
| | $O_{Water}$–$HC_{Methyl}$ | 2.456 | 2.952 | 0.496 | 121.30 | 131.52 | | |
| PA–$2H_2O$ | | | | | | | | |
| Tc–$2H_2O$ | $OH_{Carboxylic}$–$O_{Water1}$ | 1.728 | 1.650 | -0.078 | 169.90 | 162.27 | 0.00 | 0.00 |
| | $OH_{Water1}$–$O_{Carbonyl}$ | 2.053 | 2.489 | 0.436 | 128.72 | 105.93 | | |
| | $O_{Carboxylic}$–$HO_{Water2}$ | 1.917 | 1.890 | -0.027 | 164.49 | 177.87 | | |
| | $O_{Water2}$–$HC_{Methyl}$ | 2.446 | 3.044 | 0.598 | 127.89 | 106.05 | | |
| Ct–$2H_2O$ | $OH_{Carboxylic}$–$O_{Water1}$ | 1.713 | 1.599 | -0.114 | 159.68 | 174.86 | 1.82 | -1.83 |
| | $O_{Carboxylic}$–$HO_{Water1}$ | 2.105 | 3.228 | 1.123 | 128.45 | 90.89 | | |
| | $O_{Carbonyl}$–$HO_{Water2}$ | 2.762 | 2.804 | 0.042 | 110.24 | 103.48 | | |
| | $O_{Carboxylic}$–$HO_{Water2}$ | 2.006 | 1.883 | -0.123 | 175.71 | 166.60 | | |
| Tt–$2H_2O$ | $OH_{Carboxylic}$–$O_{Water}$ | 1.704 | 1.685 | -0.019 | 150.70 | 150.64 | 0.26 | 0.64 |
| | $O_{Carboxylic}$–$HO_{Water}$ | 3.095 | 3.397 | 0.302 | 94.86 | 83.79 | | |
| | $O_{Carbonyl}$–$HO_{Water}$ | 1.997 | 2.111 | 0.114 | 164.91 | 169.55 | | |
| | $O_{Water}$–$HO_{Water}$ | 1.875 | 1.878 | 0.003 | 159.39 | 160.93 | | |

[a] *Change in H-bond length from gas to aqueous phase:* $\Delta distance = distance_{aq} - distance_{gas}$

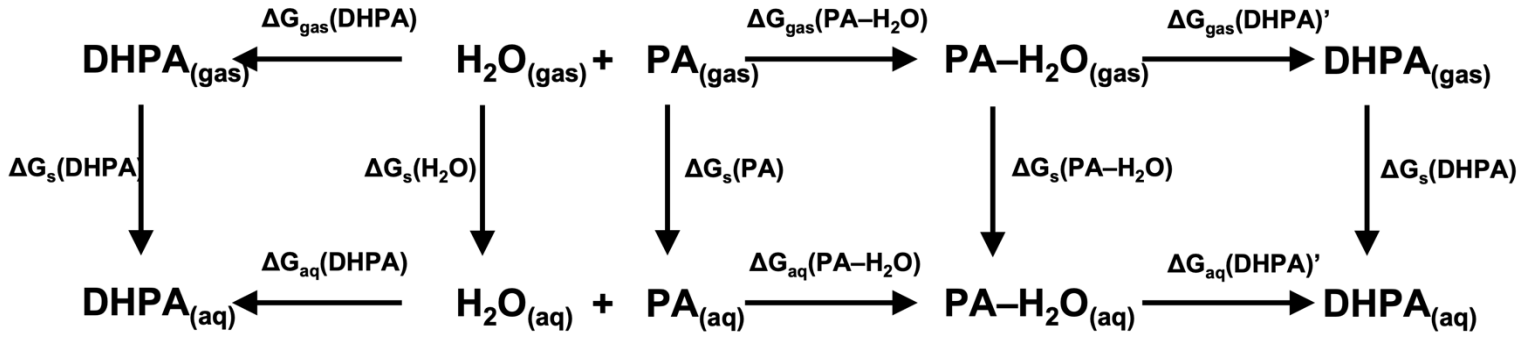


**Scheme S1A.**

**Scheme S1A.** Thermodynamic cycle of pyruvic acid (PA) monohydration to 2,2-dyhydroxypropanoic acid (DHPA) from PA–$H_2O$.

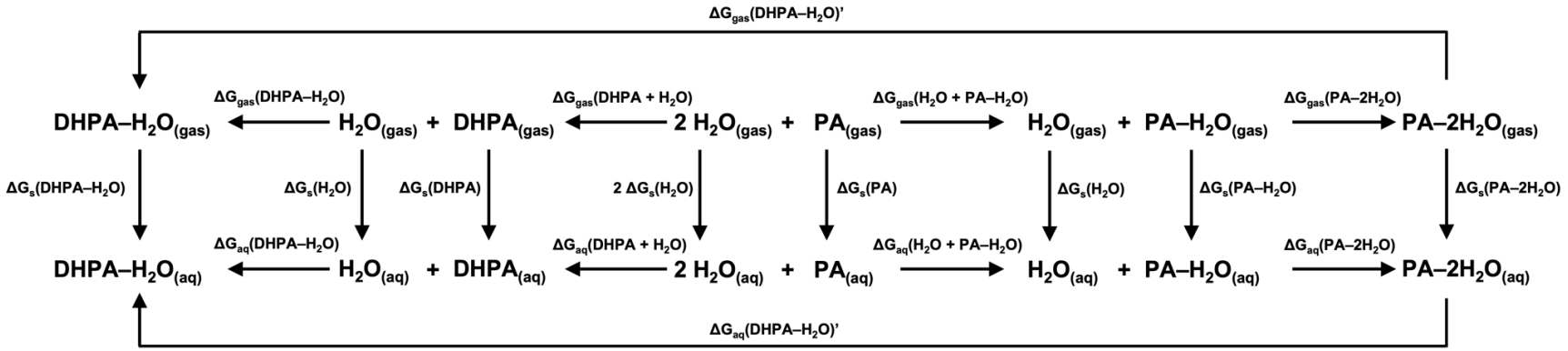


**Scheme S2A.** Thermodynamic cycle of pyruvic acid (PA) dihydration to 2,2-dyhydroxypropanoic acid (DHPA)–$H_2O$ from PA–$2H_2O$ complexes.

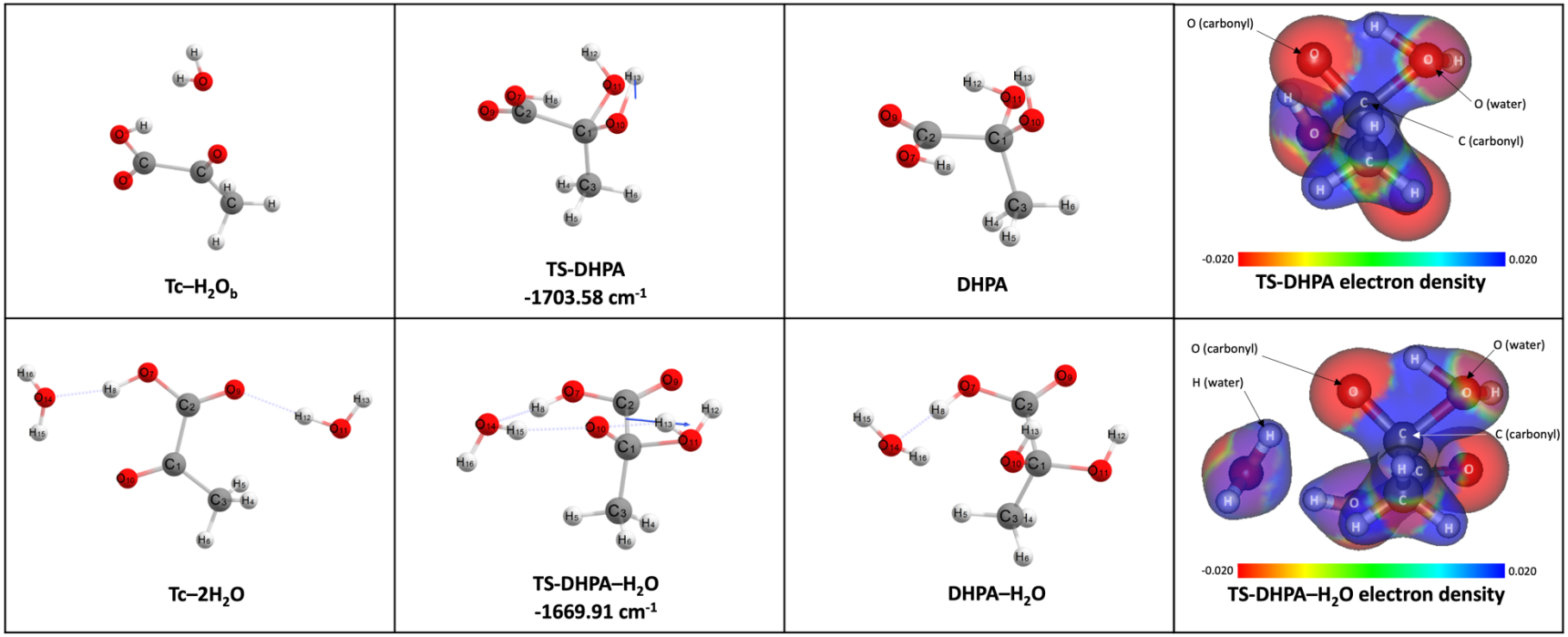


**Fig. S13A** Minima and transition state structures along the potential energy surface of 2,2-dihydroxypropanoic acid (DHPA) formation from mono- (Top) and dihydrated Tc (bottom), calculated using SMD-B2PLYP-D3BJ/aug-cc-pVTZ. Imaginary frequencies of the transition states are also indicated. Shown on the rightmost panels are the electron density map of the transition state structures. Energies of the structures are shown in Table 6.